Aalborg Universitet

AALBORG UNIVERSITY
DENMARK

Reactive power influence on the thermal cycling of multi-MW wind power inverter

Ma, Ke; Liserre, Marco ; Blaabjerg, Frede

Link to publication from Aalborg University

Reactive Power Influence on the Thermal Cycling of Multi-MW Wind Power Inverter

Ke Ma[1], Marco Liserre[2], Frede Blaabjerg[1]

[1] Department of Energy Technology, Aalborg University
Pontoppidanstraede 101, DK-9220 Aalborg East, Denmark
kema@et.aau.dk, fbl@et.aau.dk

[2] Dept of Electrotechnical and Electronic Engineering, Polytechnic of Bari
Via E.Orabona 4, 70125 - Bari, Italy
liserre@poliba.it

Abstract—**In this paper the reactive power influence on the thermal cycling of power devices in grid-connected inverter for 10 MW wind turbines is investigated. Restrained by the grid codes, the allowable reactive power ranges in relation to amplitude and phase angle of the load current for a single converter system are first presented at different wind speeds. Furthermore, the interaction between paralleled converter systems in a wind park is also considered and analyzed. By controlling the reactive power circulated among paralleled converters, a new concept is then proposed to stabilize the thermal fluctuation of the power devices during wind gusts. It is concluded that the reactive power may change the thermal distribution of power devices. By properly controlling the reactive power, it is possible to achieve a more stable junction temperature in the power devices during the fluctuation of wind speed, and thereby could provide a new way to improve the reliability of the wind power conversion system.**

I. INTRODUCTION

The European Union has committed itself to source 20% of its energy from renewables by 2020 [1]. As the most promising candidate, the wind energy production integrated into the power grid is booming up all over the world. Meanwhile, the power capacity of a single wind turbine is increasing continuously to reduce the price pr. produced kWh, as the cutting-edge achievement, 7 MW offshore wind turbines have already been presented on the market [2]-[4]. Consequently, due to much more significant impacts to the power grid than ever before, the wind power generation system is required to be more reliable and able to withstand some environment or grid disturbances.

The growing requirements for reliability and grid integration push the solutions of wind power generation system from Doubly Fed Induction Generator (DFIG) with partial-rated power converter to Synchronous or Asynchronous Generator with full-scale power converter. In the full-scale power converter solutions, there are more flexibilities to control the reactive power, and it is easier to satisfy the grid voltage support requirements by most of the grid standards under both normal and faults operation of the power grid [5], [6].

However, the added reactive power, especially in the application of multi-MW wind power conversion, will increase the converter output voltage (modulation index) and change the amplitude as well as phase angle of the load current in the grid side inverter, as shown in Fig. 1, where the voltage and current phasor diagram when introducing the overexcited and underexcited reactive current I_Q to a grid connected converter are indicated respectively. Referring to the commonly used and accepted loss model in [7], the modified output voltage and load current will change the loss

(a) Overexcited reactive power (I_{Q+}).

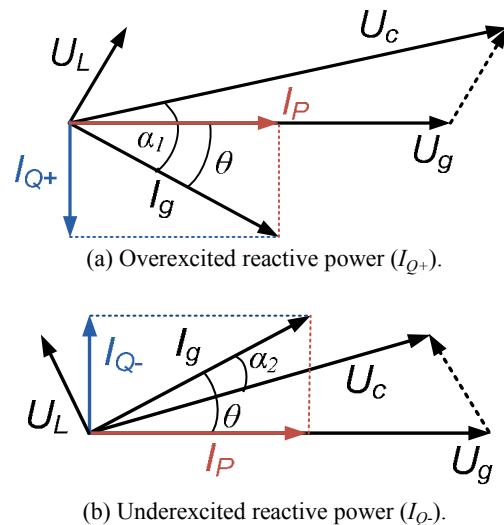(b) Underexcited reactive power (I_{Q-}).

Fig. 1. The phasor diagram of grid side inverter by introducing reactive power (U_c represents the converter output voltage, U_g grid voltage, U_L voltage drop on filter inductor, I_g load current, I_P active current, I_Q reactive current, $cos\theta$ power factor, α the phase angle).

consumption and distribution, and thereby lead to the change of thermal cycling (or junction temperature) of power switching devices. According to most of the reliability models for power semiconductors [8]-[10], the life time of the wind power inverter is closely related to the thermal cycling performance, therefore it is interesting to investigate the relationship between the reactive power and the resulting modified thermal cycling for multi-MW wind power inverter.

In this paper, the allowable reactive power ranges as well as their impacts on thermal cycling of wind power inverters are presented at different wind speeds, and situations when considering single converter and paralleled converter systems in a wind park are analyzed respectively. A new concept is also proposed to stabilize the device thermal fluctuation during wind gust by controlling the reactive power circulated among parallel converter systems.

II. EFFECT OF REACTIVE POWER IN CASE OF SINGLE CONVERTER

As the most commercialized multilevel topology which is widely used in the high-power medium-voltage drives for industry, mining, and traction applications [11]-[14], the three-level neutral-point-clamped (3L-NPC) converter seems to be a promising candidate for the Multi-MW full-scale wind power conversion system [10]-[14], as shown in Fig. 2, this converter is chosen and basically designed based on a 10 MW wind turbine as a case study [15]-[18], where the major parameters are summarized in Table I.
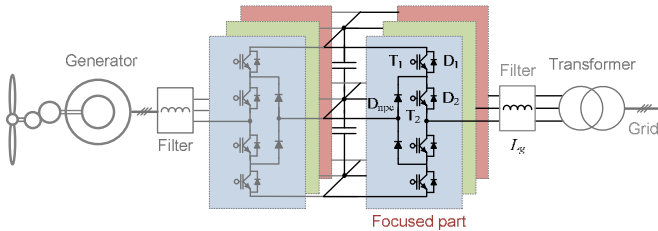

Fig. 2. Three-level Neutral point clamped converter used in a wind turbine.

Table I. Parameters of three-level Neural Point Clamped inverter for case study

Rated active power P	10 MW
DC bus voltage V_{dc}	5.6 $kV\ DC$
[1] Rated primary side voltage V_{ll}	3.3 $kV\ rms$
[2] Rated phase current I_{phase}	1.94 $kA\ rms$
Carrier frequency f_c	800 Hz
Filter inductance L_f	1.13 mH (0.3 $p.u.$)

1. Line-to-line voltage in the primary windings of the transformer.
2. Phase current when power factor is 0.9.

For a single wind power generation system, the maximum reactive power achieved by the grid side inverter has to be restrained in a certain range according to the grid standards [5]-[6], as shown in Fig. 3, in which the allowable boundaries of reactive power with relation to the generating active power is defined by German grid code. It can be seen that in the definition of Variant 1 the overexcited reactive power Q_+ should be less than 48% of the active power P, and the underexcited reactive power Q- should be less than 23% of P.
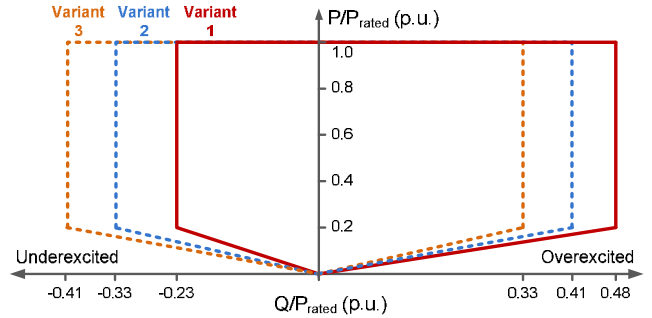

Fig. 3. The P, Q range of wind power converter during normal operation defined by the German grid codes [6].

Referring to the phasor diagram of the grid side converter in Fig. 1, the amplitude of load current I_g with relation to the reactive power Q and active power P can be calculated as:

$$I_g = \frac{\sqrt{P^2 + Q^2}}{3 \cdot U_g} \quad (1)$$

Where U_g is the rms value of grid phase voltage. The phase angle α between load current I_g and converter output voltage U_c in Fig. 1 can be calculated as:

$$\alpha_1 = \arctan\left[\frac{U_g \cdot \sin\theta + 2\pi f_o L_f \cdot I_g}{U_g \cdot PF}\right] \quad (2)$$

when introducing overexcited reactive power, and

$$\alpha_2 = -\arctan\left[\frac{U_g \cdot \sin\theta - 2\pi f_o L_f \cdot I_g}{U_g \cdot PF}\right] \quad (3)$$

when introducing underexcited reactive power.

In (2) and (3), the power factor angle θ is:

$$\theta = \arccos\frac{P}{\sqrt{P^2 + Q^2}} \quad (4)$$

Considering the grid code defined in Fig. 3, the restrained condition has to be added as:

$$-0.23P \leq Q \leq 0.48P \quad (5)$$

given the condition that generating active power P is larger than 20% of its rated value.

Then the amplitude and phase angle of the load current I_g in relation to the reactive power p.u. can be plotted in Fig. 4 (a) and Fig. 4 (b) respectively, in which the situations when

the wind speed is 12m/s (P = 10 MW), 10 m/s (P = 6.3 MW), and 8 m/s (P = 3.2 MW), are indicated.
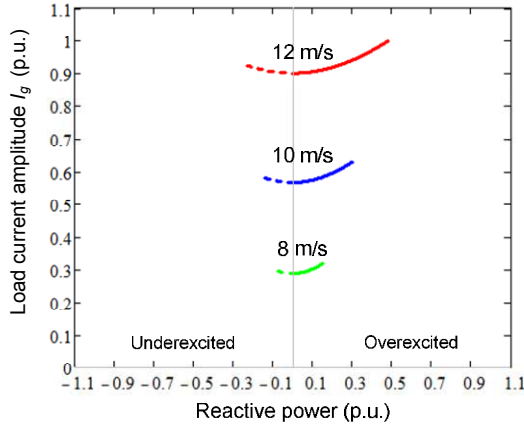
(a) Current amplitude I_g vs. reactive power Q
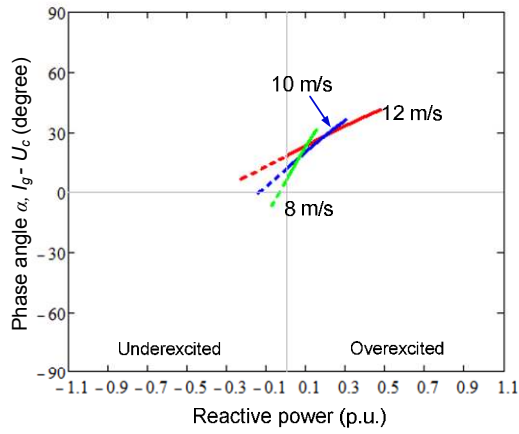
(b) Phase angle α vs. reactive power Q

Fig. 4. Load current vs. reactive power when complying with grid codes (dot line represents underexcited Q_-, real line represents overexcited Q_+).

In order to investigate the maximum impacts of the reactive power to the losses and find the thermal distribution of power devices, three extreme conditions when complying with grid codes are chosen based on 10 m/s wind speed from Fig. 4 (10 m/s is the typical average annual offshore wind speed defined by IEC I wind class standard [19]): the maximum underexcited reactive power boundary when Q_{-max} $_{(10\ m/s)}$ = -0.13 p.u., no reactive power when PF = 1, and maximum overexcited reactive power boundary when Q_{+max} $_{(10\ m/s)}$ = 0.27 p.u..

The loss model shares the same idea in [7], which is a commonly accepted method for loss evaluation of power semiconductor devices, the conduction loss and switching loss are acuminated by switching cycles according to the information of conduction voltage as well as switching energy in relation to the load current provided by the datasheets of manufacturers. The simulation is carried out based on PLECS Blockset in Simulink. Press-pack IGCT

5SHY35L4512 (commutated voltage 2.8 kV/ maximum current 3.3 kArms) and diodes 5SDF16L4503 (2.8 kV/2.6 kArms) from ABB are chosen as the power switching devices. For simplicity losses dissipated in the devices are considered as temperature independent.

The thermal models of a single switch and clamped diode are indicated in Fig. 5 [8], [20], in which the thermal impedance from junction to case $Z_{(j-c)}$ is modeled as a four-layers Foster RC network, as shown in Fig. 6. Each of the thermal parameters can be found from the manufacturer datasheets and they are summarized in Table II, where the thermal resistance R_{th} will decide the steady state mean value of junction temperature, and the thermal capacitance (with time constant τ) will decide the dynamic change or fluctuation of the junction temperature. The ambient temperature is set to 50 ℃ and considered constant during the operation of converter, however it may be changed depends on the operation site.
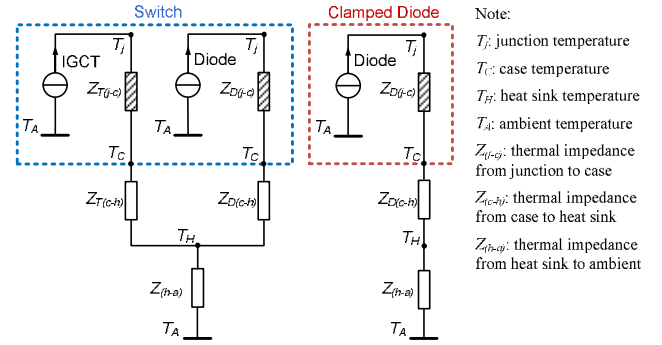

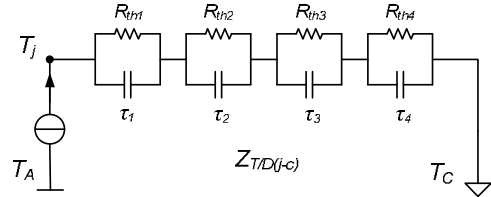Fig. 5. Thermal models of the power devices.

Fig. 6. Thermal model of the impedance $Z_{T(j-c)}$ or $Z_{D(j-c)}$ from junction to case in Fig. 5.

Table II. Parameters of thermal impedance for IGCT/diode.

Thermal Impedance	$\mathbf{Z_{T/D(j-c)}}$				$\mathbf{Z_{T/D(c-h)}}$
	Sector 1	Sector 2	Sector 3	Sector 4	
R_{iIGCT} (K/kW)	5.562	1.527	0.868	0.545	3
τ_{iIGCT} (s)	0.5119	0.896	0.0091	0.0024	-
R_{iDiode} (K/kW)	11.124	3.054	1.736	1.09	6
τ_{iDiode} (s)	0.5119	0.896	0.0091	0.0024	-

*Sector N means different layers of thermal RC lump in Fig. 6.

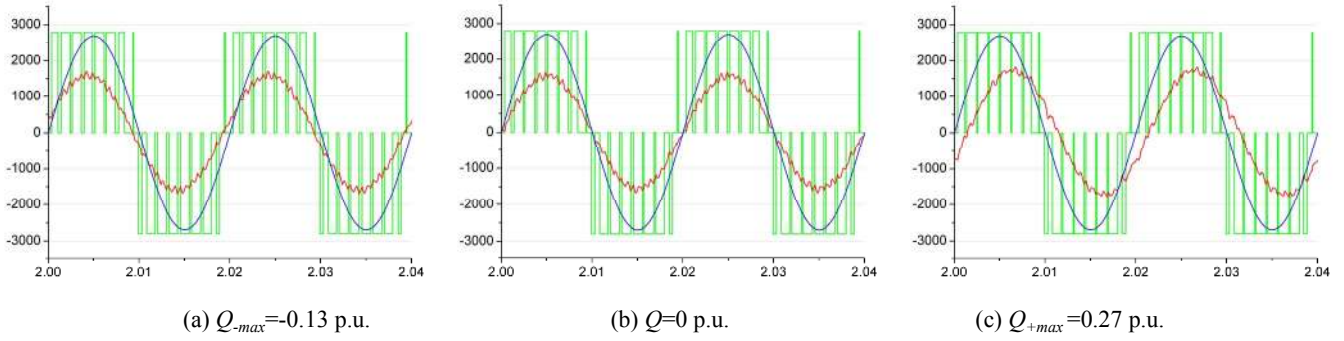(a) Q_{-max}=-0.13 p.u.   (b) Q=0 p.u.   (c) Q_{+max}=0.27 p.u.

Fig. 7. Output waveforms of 3L-NPC inverter under different reactive power (boundaries defined by grid codes, 10 m/s wind speed), output voltage pulses (Green), grid voltage (blue), phase current (red).
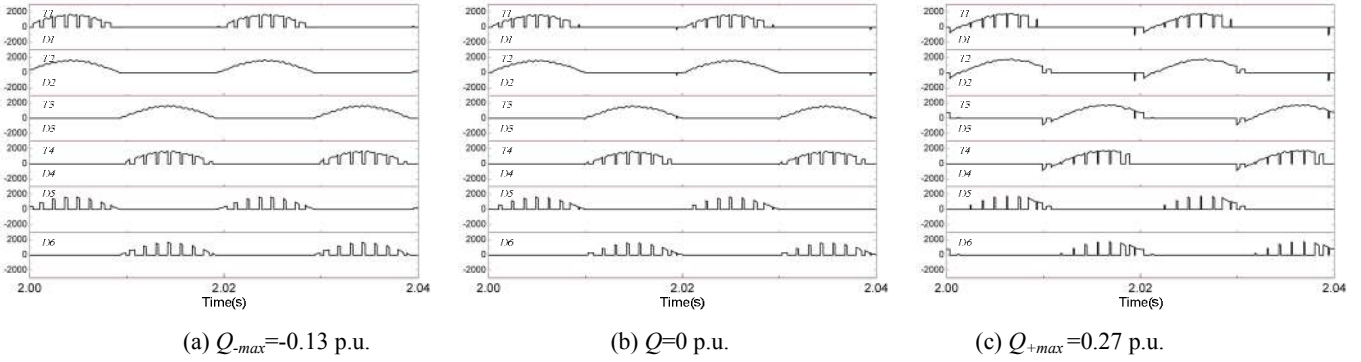

(a) Q_{-max}=-0.13 p.u.   (b) Q=0 p.u.   (c) Q_{+max}=0.27 p.u.

Fig. 8. Current distribution of 3L-NPC inverter under different reactive powers (boundaries defined by grid codes, 10 m/s wind speed).

(a) Q_{-max}=-0.13 p.u.   (b) Q=0 p.u.   (c) Q_{+max}=0.27 p.u.
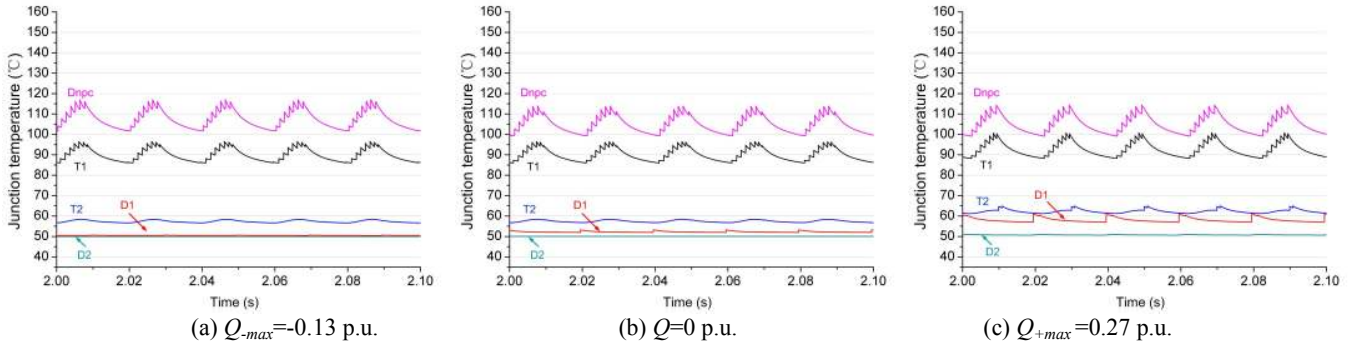
Fig. 9. Thermal cycling of 3L-NPC inverter under different reactive powers (boundaries defined by grid codes, 10 m/s wind speed).

It is noted that the separately packaged IGCT and diodes are chosen because of the limitation for available products which can be found on the market. However, in a practical converter design, the IGCT/IGBT and its freewheeling diode are usually integrated and packaged together, the chip size for diode is about half of that for the IGCT/IGBT, accordingly, the thermal resistance of the diode from junction to heat sink is not consistent with its datasheet values but set to twice of the IGCT. In Mega-Watts power converter systems, separated heat sink is typically used, a good thermal decoupling among the power devices can be achieved, so the thermal resistance between heat sink and ambient is considered small.

The simulation results regarding inverter outputs and current distribution are shown in Fig. 7 and Fig. 8 respectively, where the three extreme reactive power conditions are introduced to the inverter when generating 0.63 p.u. active power at 10 m/s wind speed. It can be seen that when complying with the regulations by grid codes, the differences of converter outputs with the given three extreme reactive powers are insignificant.

The loss simulation results of the 3L-NPC wind power inverter are presented in Fig. 10, in which three given reactive power conditions are compared. It can be seen that there is no significant loss difference between the three conditions where different amount of reactive power are introduced. The situation at the maximum overexcited reactive power boundary (Q_{+max} = 0.27 p.u.) consumes slightly more loss in the outer switches and diode T1, D1 and inner switch T2 of the 3L-NPC inverter.
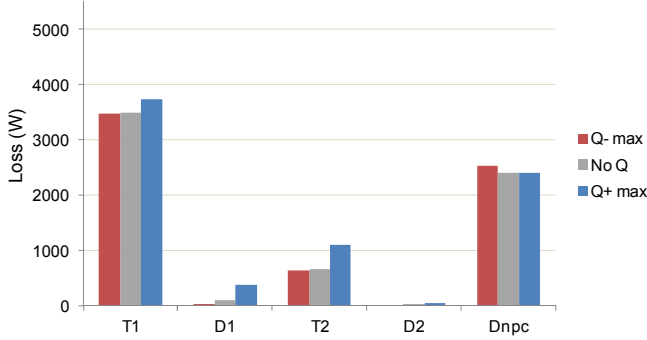
Fig. 10. Loss distribution of 3L-NPC inverter with different extreme reactive powers (Complying with grid codes).

According to the junction temperature simulation results in Fig. 9, the thermal cycling in the most stressed devices of the clamping diode Dnpc as well as the outer switches T1 has no significant difference among the three reactive power operating points.

III. EFFECT OF REACTIVE POWER IN CASE OF PARALLELED CONVERTERS

For wind power converter systems in a wind farm, the grid side inverters are connected as a local grid, therefore the reactive power can basically be circulated among the inverters locally and not necessarily be seen in the power grid, as shown in Fig. 11. On this condition the operation range of reactive power is not restrained by the grid codes but by the amplitude of load current as well as the converter output voltage, which is due to the limitations of device current rating and maximum modulation index of the power converter.
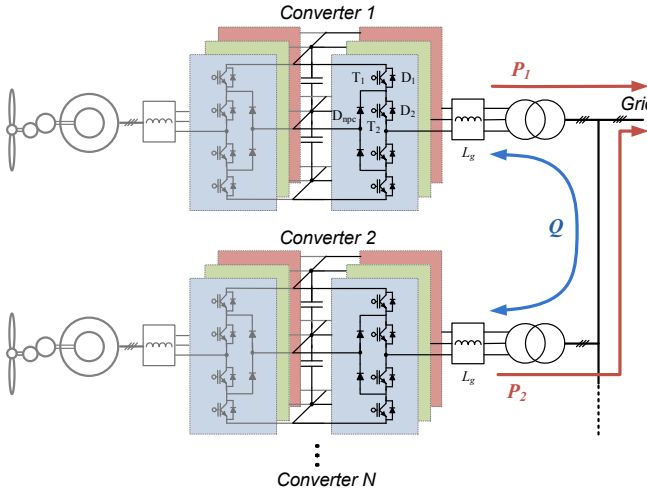

Fig. 11. Reactive power circulated in paralleled wind power converters.

The new ranges of amplitude and phase angle of the load current with relation to the reactive power are shown in Fig. 12, which is restrained by:

$$-\sqrt{S^2 - P^2} \leq Q \leq \sqrt{S^2 - P^2} \qquad (6)$$

$$M \leq 1 \qquad (7)$$

where the modulation index M can be calculated as:

$$M = \frac{\sqrt{6} \cdot U_c}{V_{dc}}$$

$$= \frac{\sqrt{6} \cdot \sqrt{(U_g \cdot PF)^2 + [U_g \cdot \sin\theta \pm 2\pi f_o \cdot L_f \cdot I_g]^2}}{V_{dc}} \qquad (8)$$

It can be seen that the operating range of reactive power is significantly extended compared to Fig. 4, and the ranges for overexcited and underexcited reactive current are unsymmetrical: The increase of Q_+ will cause an increase of converter output voltage U_c, therefore the Q_+ is first limited by the maximum modulation index before it gets to the limitation of maximum device current rating. While the increase of Q_- will cause a decrease of U_c and the modulation index, therefore Q_- is only limited by the device current rating.
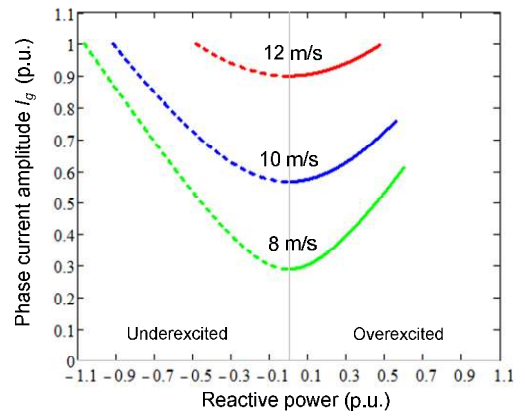
(b) Current amplitude I_g vs. reactive power Q
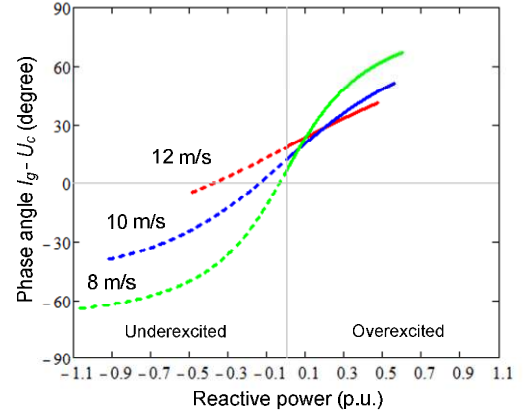
(a) Phase angle α vs. reactive power Q

Fig. 12. Operation range of reactive power when complying with grid codes (dot line represents underexcited Q_-, real line represents overexcited Q_+).

Another three extreme reactive power conditions when considering the interaction between paralleled converters are investigated based on 10 m/s wind speed: the maximum underexcited reactive power boundary when $Q_{-max\ (10m/s)}$=-0.82 p.u., no reactive power when PF=1, and maximum

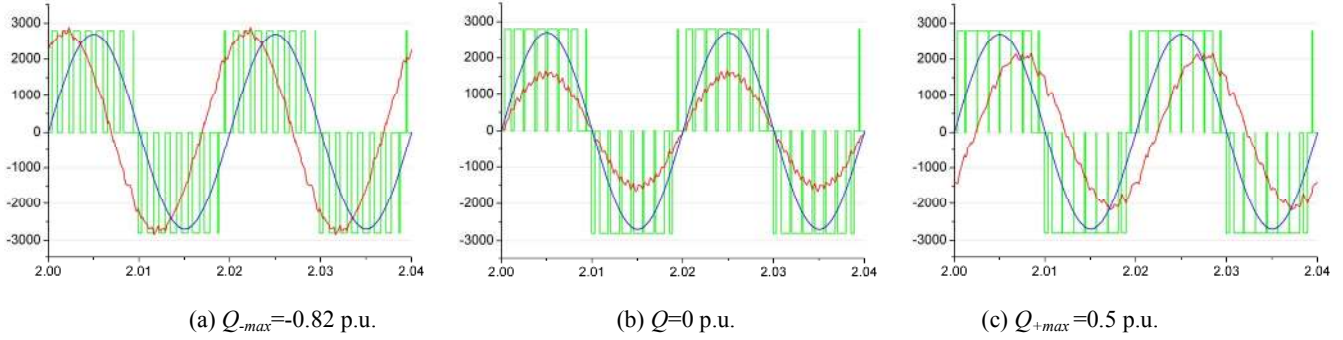(a) Q_{-max}=-0.82 p.u. (b) Q=0 p.u. (c) Q_{+max}=0.5 p.u.

Fig. 13. Output waveforms of 3L-NPC inverter under different reactive power (Considering interaction of inverters, 10 m/s wind speed), output voltage pulses (Green), grid voltage (blue), phase current (red).
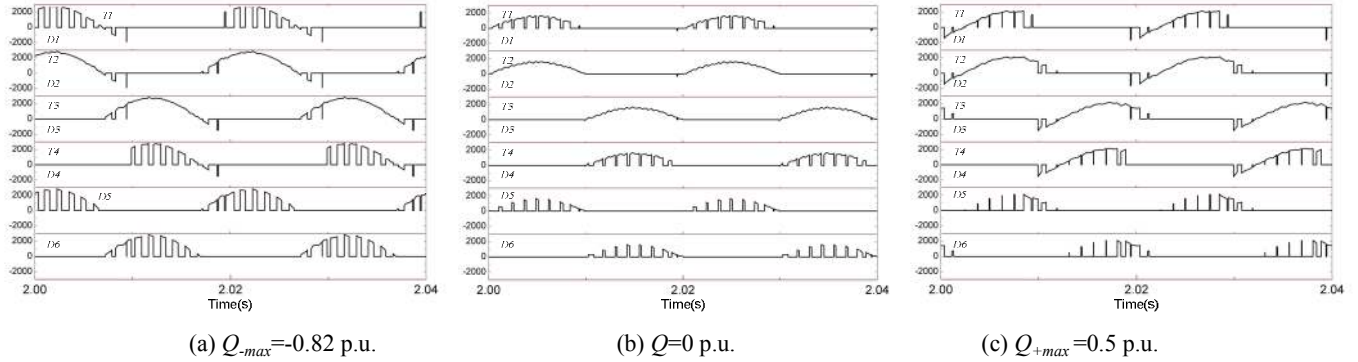

(a) Q_{-max}=-0.82 p.u. (b) Q=0 p.u. (c) Q_{+max}=0.5 p.u.

Fig. 14. Current distribution of 3L-NPC inverter under different reactive powers (Considering interaction of inverters, 10 m/s wind speed).

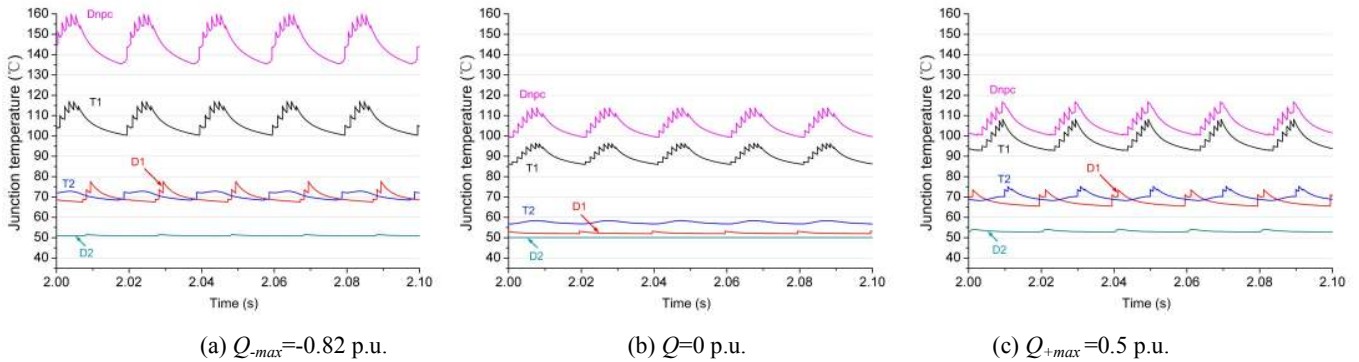(a) Q_{-max}=-0.82 p.u. (b) Q=0 p.u. (c) Q_{+max}=0.5 p.u.

Fig. 15. Thermal cycling of 3L-NPC inverter under different reactive powers (Considering interaction of inverters, 10 m/s wind speed).

overexcited reactive current boundary when $Q_{+max\ (10\ m/s)}$=0.5 p.u..

The simulation results regarding inverter outputs and current distribution are shown in Fig. 13 and Fig. 14 respectively, where the three extreme reactive power conditions are introduced when generating 0.63 p.u. active power at 10 m/s wind speed. It can be seen that when considering the interaction between paralleled converters, the converter output pulse width, amplitude and phase angle of load current with the given three extreme reactive powers significantly differ from each other.

The loss simulation results are presented in Fig. 16, in which three given reactive power conditions are compared when the interaction between parallel converters are considered. It can be seen that the situation at maximum

overexcited reactive power boundary (Q_{+max} =0.5 p.u.) consumes significant more loss than the situation without reactive power in the outer switches T1, outer diode D1, inner switch T2 and clamping diode D_{npc} of the 3L-NPC inverter. The major difference between overexcited and underexcited reactive power boundary is at the stress of the clamping diode, the later has much less loss than the former one in Dnpc.

According to the junction temperature simulation results in Fig. 15, the thermal cycling of the most stressed device of the clamping diode Dnpc as well as outer switche T1 is significant higher than the other two reactive power operating points.
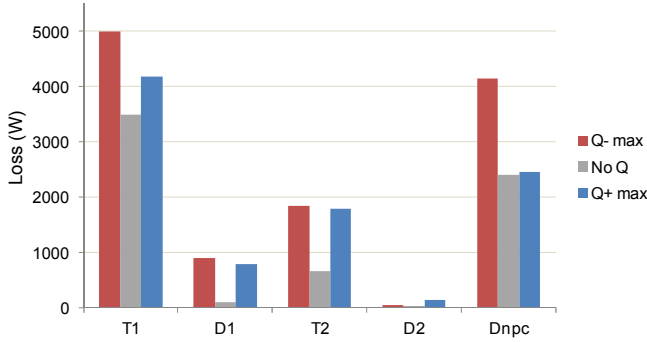
Fig. 16. Loss distribution of 3L-NPC inverter with different extreme reactive powers (Considering parallel converters).

IV. REACTIVE POWER CONTROL METHOD TO STABLIZE THE THERMAL CYCLING

It can be seen that when considering the interaction among parallelled inverters, the underexcited reactive current may introduce significantly increased junction temperature in the most stressed devices (outer switches T1 and clamping diode Dnpc). This feature can be utilized to stabilize the fluctuation of the power device junction temperature (especially during the change of wind speed), which may be harmful to the reliability of the converter system as claimed in [8]-[10].

According to the one year return period wind gust definition by IEC standards [19], a wind gust condition with different reactive current references for case study are indicated in Fig. 17 (the wind speed is set from 10 m/s dropping to 8 m/s and rising to 16 m/s, then the reverse

fashion is continued). The active current reference of converter is accordingly changed with the wind speed referring to the wind turbine model in [18], while the reactive power references are different: Fig. 17 (a) is the situation without any reactive current during the wind gust. Fig. 17 (b) enable the reactive power control strategy which adjust the amount of underexcited reactive current to keep the mean value of junction temperature in the most stressed device (Dnpc) constant when the wind speed is below 11 m/s, and the reactive current is kept zero when the wind speed is above 11m/s to avoid over heat of the most stress device. The basic idea and used models for calculating the active and reactive current references is shown in Fig. 19.
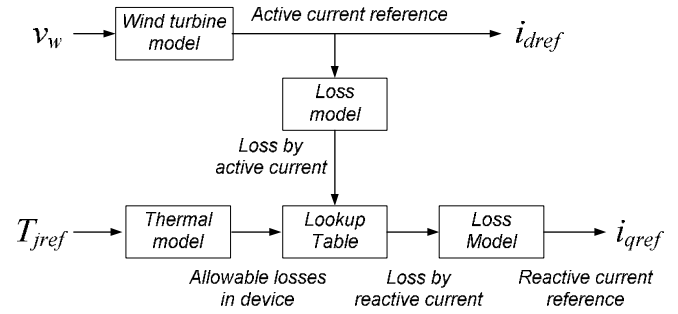

Fig. 19. The basic idea and used models for calculating the active and reactive current references of Fig. (b). (v_w is the wind speed, T_{jref} is the target junction temperature mean value to be stablized in the most stressed devices.)

Fig. 17 (c) is the situation with overexcited reactive current. This reactive power control strategy is conducted on the other parallelled converter(s) to compensate the

(a) Without reactive power   (b) With underexcited reactive power   (c) With overexcited reactive power
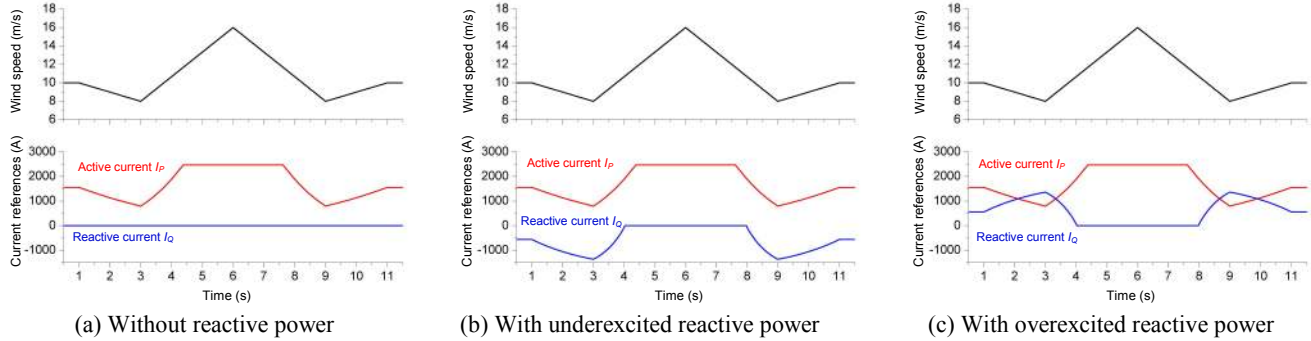
Fig. 17. Wind gust and current references of 3L-NPC inverter for case study.

(a) Without reactive power   (b) With underexcited reactive power   (c) With overexcited reactive power
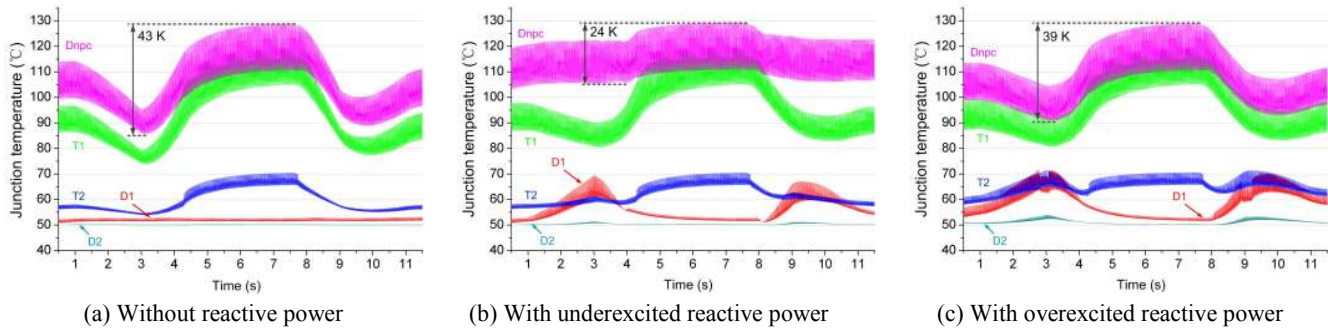
Fig. 18. Thermal cycling of 3L-NPC inverter during wind gust.

underexcited reactive power generated by the converter with references in Fig. 17 (b), so the overexcited reactive current reference in Fig. 17 (c) has the same amplitude but different direction compared to Fig. 17 (b).

The junction temperature distribution of the target 3L-NPC inverter with different reactive current control strategies are indicated in Fig. 18. It is obvious that the thermal fluctuations in the most stressed devices (clamping diode Dnpc) are significantly reduced from 43 K in Fig. 18 (a) without reactive power to 24 K in Fig. 18 (b) with the underexcited reactive power control. And it can be seen that when conducing the reactive power compensation in paralleled converter with overexcited reactive current reference in Fig.18 (c), the maximum junction temperature in the most stressed devices Dnpc is not further more increased.

However, when introducing reactive power (either overexcited or underexcited) to the 3L-NPC inverter, the outer diode D1, inner switch T2 inner diode D2 are slightly more stressed compared to the situation without any reactive power.

CONCLUSIONS

The introduction of reactive current may change the thermal distribution of power devices. The operation ranges of reactive current not only depend on the grid codes, but also relate to the interaction between paralleled inverters-the latter situation has much wider allowable reactive current range than the former one.

By introducing reactive current during the lower wind speed of a wind gust, the junction temperature fluctuation in the most stressed devices of a 3L-NPC wind power inverter can be significantly stabilized, and the reliability could be thereby improved according to e.g. the Coffin-Masson life time models, while the increased stresses to the other devices or paralleled converters are still acceptable.

REFERENCES

[1] Z. Chen, J.M. Guerrero, F. Blaabjerg, "A Review of the State of the Art of Power Electronics for Wind Turbines," *IEEE Transactions on Power Electronics,* vol.24, no.8, pp.1859-1875, Aug. 2009.

[2] F. Blaabjerg, Z. Chen, S.B. Kjaer, "Power Electronics as Efficient Interface in Dispersed Power Generation Systems", *IEEE Transactions on Power Electronics*, 2004, vol. 19, no. 4, pp. 1184-1194.

[3] Z. Chen, J.M. Guerrero, F. Blaabjerg, "A Review of the State of the Art of Power Electronics for Wind Turbines," *IEEE Transactions on Power Electronics,* vol.24, no.8, pp.1859-1875, Aug. 2009.

[4] Website of Vestas Wind Power, Wind turbines overview, April 2011. (Available: http://www.vestas.com/)

[5] M. Altin, O. Goksu, R. Teodorescu, P. Rodriguez, B. Bak-Jensen, L. Helle, "Overview of recent grid codes for wind power integration," Proc. of OPTIM'2010, pp.1152-1160, 2010.

[6] E.ON-Netz – Grid Code. High and extra high voltage, April 2006.

[7] F. Blaabjerg, U. Jaeger, S. Munk-Nielsen and J. Pedersen, "Power Losses in PWM-VSI Inverter Using NPT or PT IGBT Devices," *IEEE Transactions on Power Electronics,* vol. 10, no. 3, pp. 358–367, May 1995.

[8] ABB Application Note: Applying IGBTs, May 2007.

[9] W. Lixiang, J. McGuire,R.A. Lukaszewski, "Analysis of PWM Frequency Control to Improve the Lifetime of PWM Inverter," *IEEE Transactions on Industrial Applications,* vol. 47, no. 2, pp. 922-929, 2011.

[10] I.F. Kovac□ević, U. Drofenik, J.W. Kolar, "New physical model for lifetime estimation of power modules," in *Proc. IPEC'10*, pp. 2106-2114, 2010.

[11] F. Blaabjerg, M. Liserre, K. Ma, "Power Electronics Converters for Wind Turbine Systems," in *Proc. of ECCE*, pp. 281-290, Sep 2011.

[12] K. Ma, F. Blaabjerg, "Multilevel Converters for 10 MW Wind Turbines," in *Proc. of EPE*, August 2011.

[13] S. Kouro, M. Malinowski, K. Gopakumar, J. Pou, L. G. Franquelo, B. Wu, J. Rodriguez, M. A. Perez, J. I. Leon, "Recent Advances and Industrial Applications of Multilevel Converters," *IEEE Transactions on Power Electronics*, vol. 57, no. 8, pp. 2553 – 2580, 2010.

[14] J. Rodriguez, S. Bernet, P. K. Steimer, I. E. Lizama, "A Survey on Neutral-Point-Clamped Inverters," *IEEE Transactions on Industrial Electronics,* vol. 57, no. 7, pp. 2219-2230, 2010.

[15] K. Ma, F. Blaabjerg, D. Xu, "Power Devices Loading in Multilevel Converters for 10 MW Wind Turbines," in *Proc. of ISIE*, pp. 340-346, June 2011.

[16] K. Ma, F. Blaabjerg, M. Liserre, "Thermal analysis of multilevel grid side converters for 10 MW wind turbines under Low Voltage Ride Through," in *Proc. of ECCE*, pp. 2117 - 2124, Sep 2011.

[17] H. Li, Z. Chen, H. Polinder, "Optimization of Multibrid Permanent-Magnet Wind Generator Systems," *IEEE Transactions on Energy Conversion,* vol. 24, no. 1, pp. 82-92, 2009.

[18] H.Polinder, F.F.A.van der Pijl, G.-J.de Vilder, P.J.Tavner, "Comparison of direct-drive and geared generator concepts for wind turbines," *IEEE Transactions on Energy Conversion,* vol. 21, no. 3, pp. 725-733, 2006.

[19] Wind turbines, part 1: Design requirements, IEC 61400-1, 3rd edition, International Electrotechnical Commission, 2005.

[20] User manual of PLECS blockset version 3.1, March 2011.